On the current conditions along the Ormen Lange pipeline path during an extreme, idealized storm passage *

Helge Avlesen † Jarle Berntsen ‡ Gunnar Furnes §

December 2002

Abstract

Ormen Lange is an offshore gas field located in the Storegga region off the Norwegian west coast. The gas will be transported on-shore for processing by means of a pipeline. Due to the abrupt topography this pipeline will have many long free spans and meet challenging hydrodynamic conditions. This report is part of a larger study which is underway, with the main goal to build up a profound knowledge on hydrodynamic phenomena in the area.

We focus on locations along a possible path for the pipeline, and in a simulation study the effects on the flow due to the passage of a very strong and idealized low pressure system. We describe how the simulation is done by using a numerical, hydrostatic, sigma co-ordinate ocean model. From the produced time series, sampled at five locations along the pipeline path, we present distributions for absolute velocity and direction at four depths near the bottom.

We demonstrate that the effect of the event can be seen all the way through the boundary layer, and present some simple statistics for the absolute velocity produced from the time series.

1 Introduction

Ormen Lange is an offshore gas field located in the Storegga region off mid-Norway in water depths from roughly 800 to 1100m. The field being considered for development under the leadership of Norsk Hydro, is located in the core of the Storegga slide that left an almost 300m long headwall at the shelf break. Extracting and transporting gas from the reservoir includes sea-bed pipeline tracks which make it essential to have good knowledge on the current conditions in the region. An extensive program is underway with analysis of data from measurements as well as numerical modeling applied to a

*This work has been supported by Norsk Hydro under contract number 5172100

†Para//ab, Bergen Center for Computational Science (BCCS), UNIFOB

‡Department of Mathematics, University of Bergen

§Norsk Hydro, Bergen

large range of scales and phenomena. See reports by Eldevik, Eliassen, Berntsen and Furnes ([4], [2] and [5]) for more background information.

In this report we will focus on the time series from one single event, the passage of a strong idealized low pressure system described in two previous reports by Eliassen [3] and Vikebø et al. [12]. The event is modeled with a fine resolution model covering a few tens of kilometers around the production site and a resolution of 400 meters. Applying a one way nesting method, this model is forced with boundary conditions produced with another model that is set up with 20 km resolution covering the Norwegian sea. By a close inspection of the model bathymetry, we pick out five locations along the pipeline path where the slope of the topography has large changes. At these locations we save time series and vertical profiles from the simulation.

It was observed that the effect of the storm event can be experienced all the way through the boundary layer at the bottom, and that the direction of the flow in the whole water column is strongly steered by the topography and direction of the wind-forcing.

2 Description of the model setup

The system of equations and the numerical σ-coordinate ocean model are described in [1]. The equations are the continuity equation for an incompressible fluid, the Reynolds averaged momentum equations horizontally, conservation equations for temperature and salinity and the UNESCO-equation of state, see [7]. The model assumes Boussinesq and hydrostatic approximation.

The model is set up for an area surrounding the Ormen Lange production site, The bottom topography is shown in Figure 1. The horizontal spatial resolution is 400m, and the vertical distribution ranges from a couple of meters near the bottom up to about 50m resolution in the middle of the water column, before it is reduced towards 7m near the surface. Figure 2 shows the distribution of vertical layers for a depth of 700m. We ran the model with 52 layers.

The initial and lateral boundary conditions for this study were produced with an external model, a 20km resolution model of the Norwegian sea. The external model was set up with climatological initial and boundary conditions. The boundary conditions were imposed through a 7 cell wide relaxation zone using a method due to Martinsen et al. [9] called the Flow Relaxation Scheme (FRS).

The model area for the external model covers the Norwegian Sea basin, Figure 3. The horizontal grid size for the external model was 20km. The vertical 30 layers were distributed according to Lynch et al. [8]. Their formula distributes the layers symmetrically around the mean depth such that a gradually finer resolution towards the surface and the bottom is obtained.

The external model was run for 240 hours with an internal 3D time step of 360s and 30 2D time steps per 3D step. Initial values of water elevation, velocity, temperature and salinity were taken from the diagnostic climatology described in [6]. At the lateral open boundaries, except at the boundary to the Baltic, the flow relaxation scheme (FRS) was implemented as for the inner model with a 7 grid cell wide zone. Climatological values of velocity, temperature, salinity, and water elevation in addition to four tidal constituents (M_2, S_2, K_1, N_2) were used to specify the lateral boundary conditions.

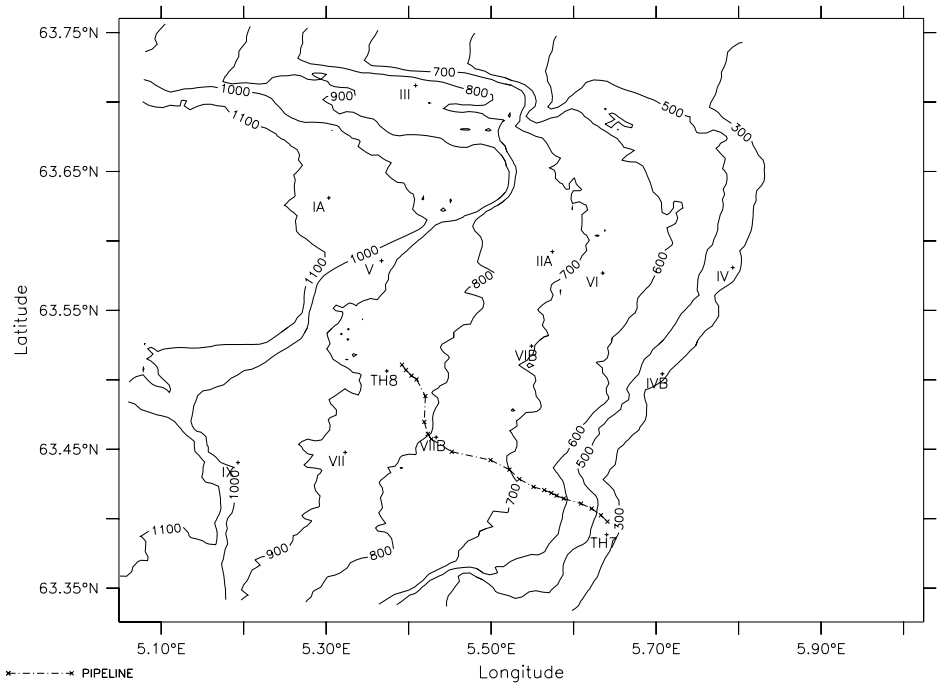


Figure 1: The bottom topography. Contour units are in meters.

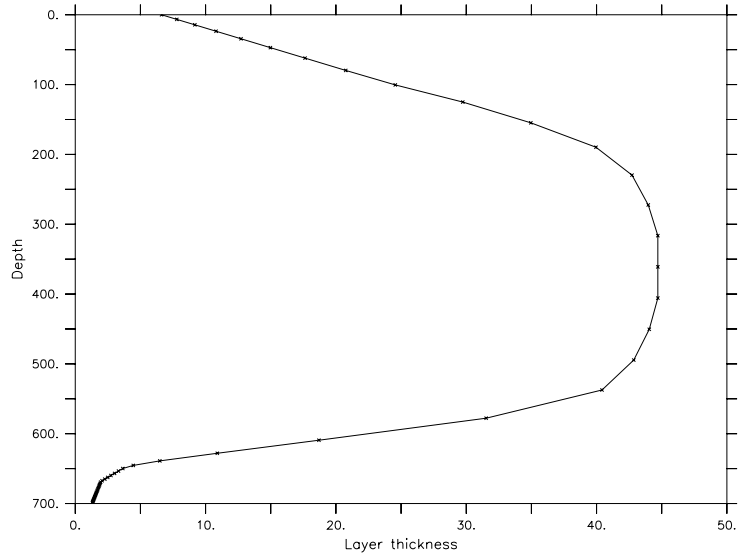


Figure 2: The distribution of layers in the vertical. All units are meters.

The flow to and from the Baltic was implemented according to an algorithm due to Stigebrandt [11]. The flow is determined from the difference in modeled water level between the southern Kattegat and the Baltic, taking climatological freshwater input to the Baltic into account. The water entering Kattegat from the Baltic is given a salinity of 8.0 p.s.u. The inflow/outflow is placed at Storebelt. Fresh water runoff from 27 rivers around the North Sea is included. For experiments over longer periods this forcing will strongly affect the coastal circulation, but in the present study this forcing has minor importance.

Traveling low pressure systems are important driving mechanisms for the oceanic flow. Martinsen et al. [10] constructed an analytical model for a cyclone and studied barotropic effects of the moving cyclone. Following Martinsen et al. the atmospheric pressure disturbance is described by

$$p(x,y,t) = p_0(t)e^{\{-[(x-x_0-u_0t)^2+(y-y_0-v_0t)^2]/R^2\}}, \tag{1}$$

where $p_0(t)$ is the pressure disturbance at the center of the cyclone; x_0, y_0 the initial position of the center of the pressure disturbance; u_0, v_0 are the x and y components of the propagation velocity; and R defines the horizontal extent of the pressure disturbance. Wind velocity components u_g and v_g in the x and y directions, respectively, are computed from the atmospheric pressure gradients as

$$u_g = -\frac{0.7}{f\rho_a}\frac{\partial p}{\partial y} \quad , \tag{2}$$

$$v_g = \frac{0.7}{f\rho_a}\frac{\partial p}{\partial x} \quad , \tag{3}$$

where f is the Coriolis parameter and ρ_a the density of the air (1.3 kg m^{-3}).

The wind stress is computed from the wind velocity components as

$$\tau_x = \rho_a c_D (u_g^2 + v_g^2)^{1/2} u_g \quad , \tag{4}$$

$$\tau_y = \rho_a c_D (u_g^2 + v_g^2)^{1/2} v_g \quad , \tag{5}$$

where c_D is the drag coefficient. In our experiments, c_D is chosen to be 3×10^{-3} following Martinsen et al. [10].

The model is first run 24 hours with $p_0(t)$ = 0. The low pressure system is then started at position $(x_0, y_0) = (-12.5, 115.84)$ and $p_0(t)$ is decreased linearly over the next 12 hours to -60hPa and held constant for the remaining simulation period, where the coordinates are the same as those in the external model of Figure 3. In the grid coordinate system, x and y components of the propagation velocities are u_0 = 8.59ms^{-1} and v_0 = -4.81ms^{-1} respectively, in all experiments.

Figure 3 is taken from Vikebø et al. [12] and shows the four trajectories that were used in a larger scale experiment with similar storms. Their results showed that the maximum velocities near the shelf break were obtained when storms with radius R=500km passed Ormen Lange along Run_track 2. The maximum velocity occurred between 70 and 80 hours after the start of the experiment. This storm was used as forcing for our model.

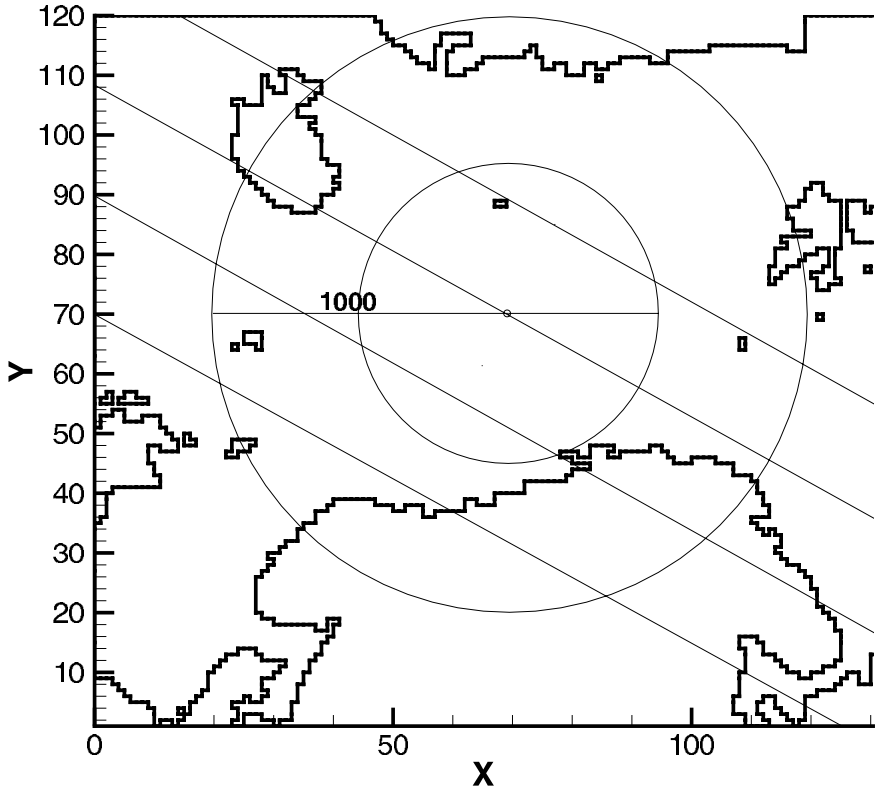


Figure 3: The horizontal extent of the model producing boundary conditions that also shows the trajectories of idealized storms, Run_track1 to Run_track4. The extension of the low pressure system indicated for $R = 1000km$ and $R = 500km$ for Run_track2. Unit of axis in grid coordinates of $20km$.

3 Results and discussion

The main limitation of this study is clearly the resolution of the topography. Figure 4 shows a detailed image of a typical part of the bottom topography around the pipeline near the tangential points TP11 to TP12. We observe that the bottom is dominated

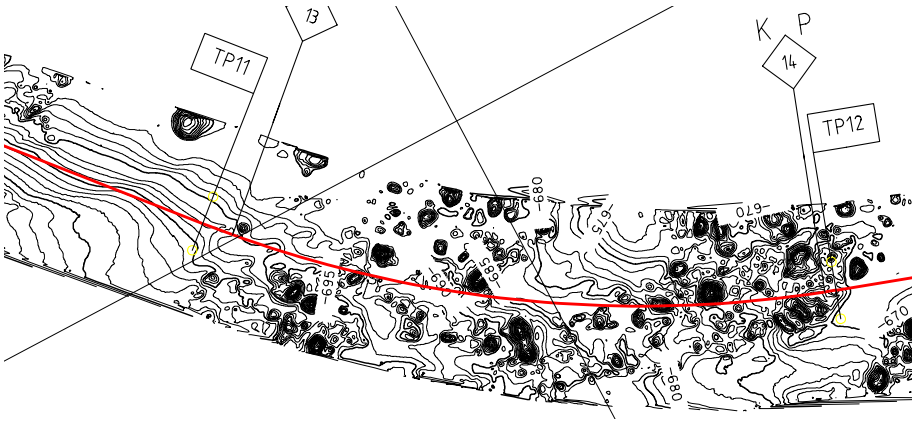


Figure 4: Detail from the Ormen Lange pipeline path at TP11-TP12 showing typical bottom topography. The distance between TP11 and TP12 is approximately 1km.

by small hills breaking up from layers of clay and mud. The horizontal extent of the hills is typically of the order of 50 meters, and the height a few tens of meters. To resolve this topography, or in other words representing the hydrodynamic effects of such topography, a numerical model would need a horizontal resolution of at least 10 meters. At the same time, the horizontal extent of the area covering the part of the pipeline we are interested in (see Figure 5) is about 30 kilometers. This would, with the ideal resolution, mean 3000 grid points in each horizontal direction – at least an order of magnitude more than we can cope with using our state of the art supercomputer equipment. We use a horizontal resolution of 400 meters, which roughly lets us cover the domain in Figure 1.

We also meet with resource limitations for the vertical direction due to the large depth of the area. By the use of a stretched coordinate system that lets us focus the effort on the surface and bottom boundary layer, we get a good resolution where assumedly most of the dynamics will happen. The distribution of layer thickness can be seen in Figure 2. It is not entirely clear how the effects of a very coarse grid in the middle of the water column will influence propagation of e.g. internal waves in the vertical, but this is beyond the scope of this report.

The tool used in the study is a free surface model. Due to the large depth of the model area, it is necessary to march forward in time using rather short time steps, in our case typically of order 2 seconds for the barotropic part of the system. The baroclinic or three dimensional part is propagated with a time step of 72 seconds. time series of velocity and temperature are sampled once per hour at the locations marked TP1 to TP20. We present results from point TP1, TP7, TP9, TP15, and TP19 since we

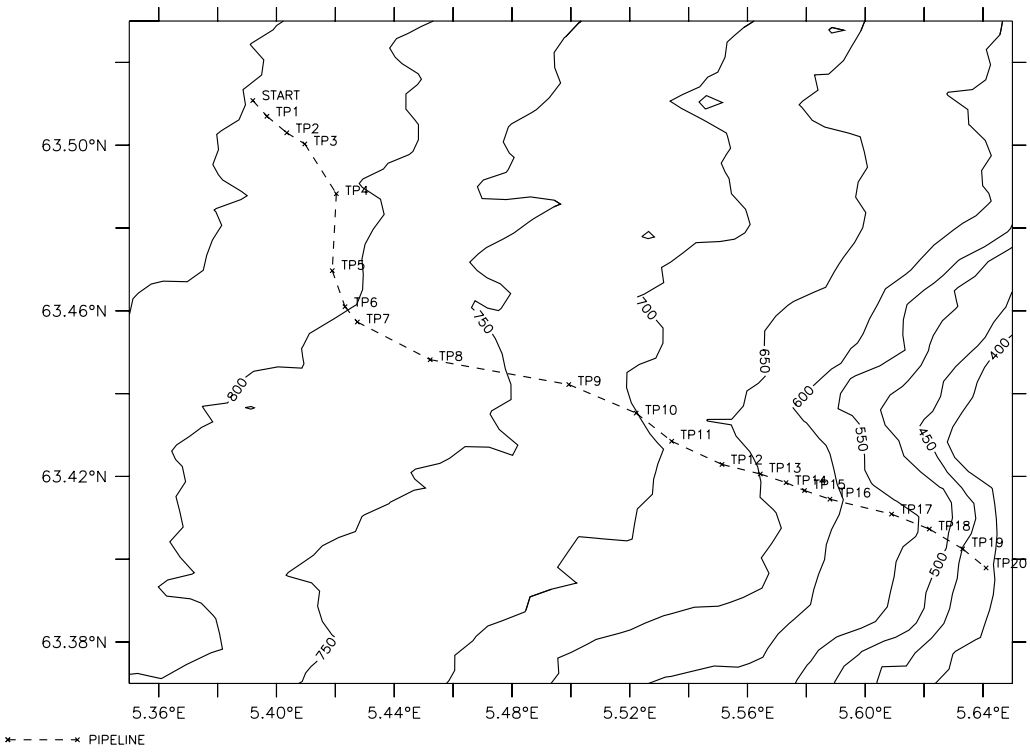


Figure 5: The model depth in meters around the pipeline path. Stations for model time series are co-located with the tangential points of the pipeline and numbered TP1 to TP20.

observe at these locations rather large changes in the slope of the model topography. It is expected that the flow will be focussed at such locations. The depths for the five stations are shown in Table 1.

Name	Long	Latt	Depth
START	5.39196	63.5108	846
TP1	5.39677	63.507	835
TP2	5.40351	63.503	826
TP3	5.40963	63.5003	829
TP4	5.42034	63.4883	818
TP5	5.41895	63.4697	811
TP6	5.42328	63.461	798
TP7	5.42747	63.4573	792
TP8	5.45222	63.4482	770
TP9	5.49929	63.4422	731
TP10	5.52219	63.4353	703
TP11	5.53424	63.4285	683
TP12	5.55135	63.4229	663
TP13	5.56435	63.4206	653
TP14	5.5731	63.4185	642
TP15	5.57937	63.4166	634
TP16	5.588	63.4145	618
TP17	5.60894	63.4109	560
TP18	5.62178	63.4073	514
TP19	5.63309	63.4025	459
TP20	5.64104	63.3979	411

Table 1: Geographical coordinates for tangential points. Depth is given in meters.

3.1 Time series of absolute velocity and temperature

Figure 6 shows the time series of absolute velocity in point TP19 for the four reference depths. The velocity peaks after about 75 hours are consistent with the external model ran separately by Vikebø et al. [12]. Since this part of the pipeline is mostly normal to the flow due to the storm, there is no significant delay between the peak velocity at the different locations, and the time series for absolute velocity at the other stations has a very similar evolution to TP19. The only difference is the magnitude of maximum velocity, which can be found in tables 2-21.

The other feature that is clearly visible in this figure is the effect of the boundary layer. The time series were sampled at depths 2,5,10 and 20 meters above the bottom, and we observe that the velocity at the 2m level is approximately 30% lower than the 50m level under the peak of the event. The boundary layer is visible throughout the whole experiment, but grows during the peak. Figures 7-9 show the evolution of the vertical profile for absolute velocity at point TP19. We observe that the bottom boundary layer is well resolved, and that the strong wind influences the flow in at least

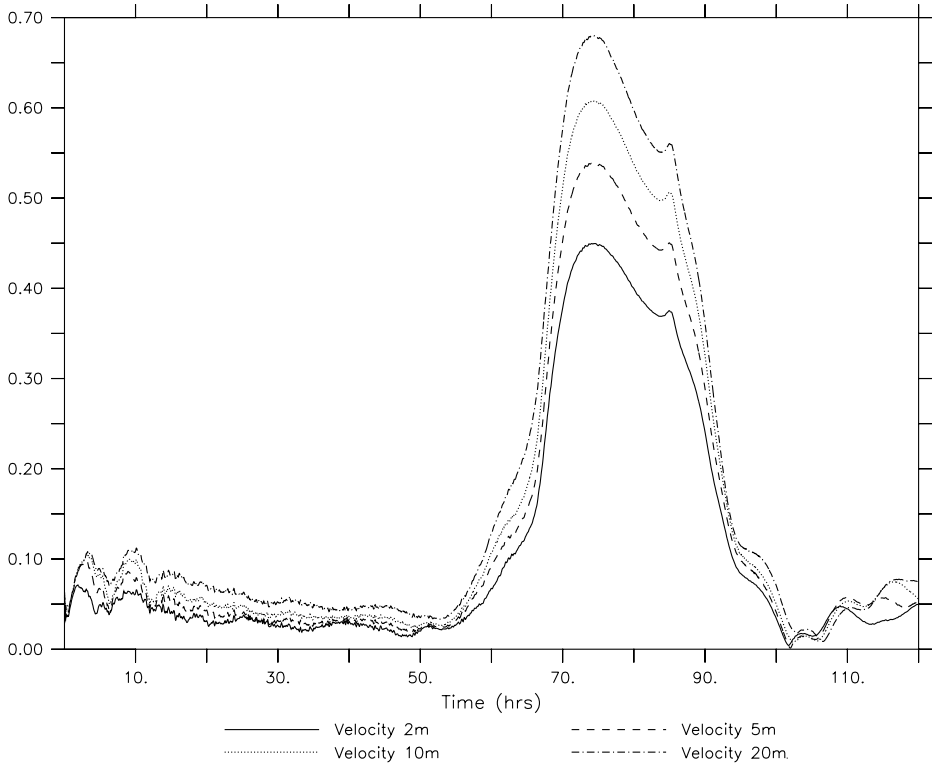


Figure 6: time series of absolute velocity at TP19 20m,10m,5m and 2m above the bottom. Unit for vertical axis is in meters, horisontal axis is in hours.

the upper 100 meters of the water column. Near the bottom we see the boundary layer grow from approximately 30m thickness to a maximum of about 60m thickness when the wind-forcing is near its maximum.

3.2 Direction and magnitude of velocity at the five stations

In Tables 2 to 21, we computed some simple statistics from the time series. The tables show a probability equal to the number of samples in a certain velocity interval and sector, divided by the total number of samples. A direction of 0 degrees means flow towards north in the model domain, while 90 degrees means eastward flow. The domain is slightly rotated with respect to geographical coordinates, about 3 degrees clockwise.

The tables generally show that the background flow with velocity up to 5-10 cm/s has large directional variability, which is reasonable due to the abrupt topography in the area. The depths for which the time series were taken are mostly inside the bottom boundary layer. This boundary layer is most likely too thin, because the model cannot represent the fine scale bathymetry we know dominate the area. This indicates that we may overestimate the velocities. On the other hand flow over fine scale features such as small sea-mounts may give increased velocities as studies with even higher resolution have shown. These uncertainties make comparison of idealized model results with real measurements difficult.

The tables show that when the velocity goes above 10-15cm/s, the direction is mostly uniform, both with respect to the velocity and the depth of the sampling point. This direction is often not (as expected) aligned with the local topography, but seems to be influenced mostly by the wind field. An example of this can be seen in Figure 10, which shows the velocity at 5 meter height above the bottom after 72 hours, very close to the peak of the storm event.

3.3 Distributions for absolute velocity at the stations

By doing simple statistical calculations on the time series, we calculated the probability density distribution and the cumulative density distribution for absolute velocity, see figures 11 to 14. The cumulative distribution for absolute velocity are curves which gives the probability that the velocity is smaller than a given value. All curves therefore end at y value equal to 1. The shape of the cumulative distributions for different depths are strikingly similar, which makes sense since the statistics is made from one event. The event is wind driven and should work on the water masses below in a similar way for the model area since the length scale of the low pressure system is much larger than the extent of the model domain. The local topography will give differences, but the model bathymetry is quite smooth due to the resolution, so the differences will be smaller than statistics for corresponding measurements.

The probability density distributions in figures 13 and 14 are curves that give the probability for the velocity to be in a certain interval that is equal to the integral of the distribution over that interval. These distributions show the event more clearly than the cumulative distributions. We observe that the background flow has the highest probability with velocities in the range 0-15cm/s. All distributions have a small “tail” in the rightmost end of the spectrum, that identifies the low pressure event. Also here

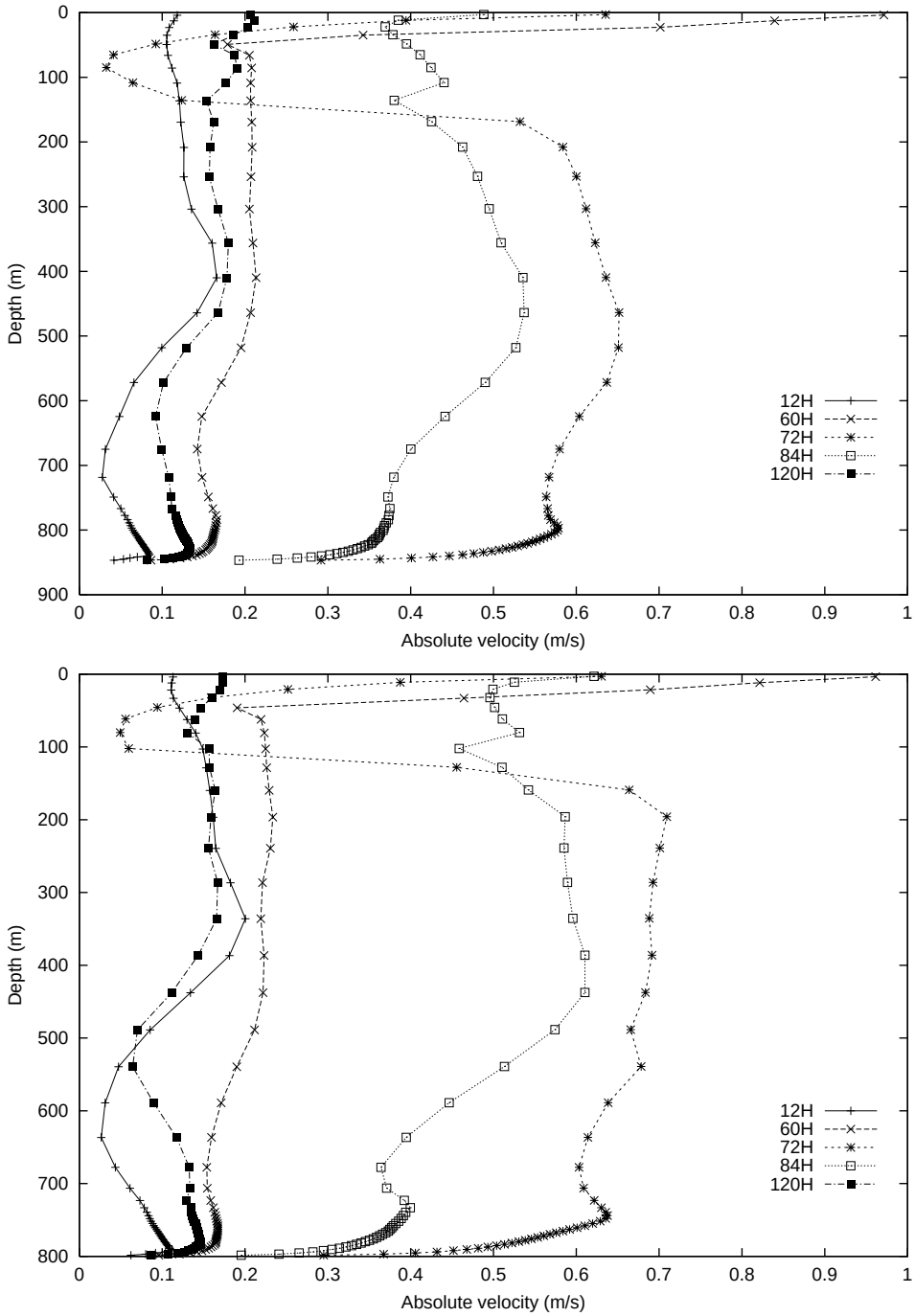


Figure 7: Time evolution of vertical profile for absolute velocity at TP1(top) and TP7(bottom)

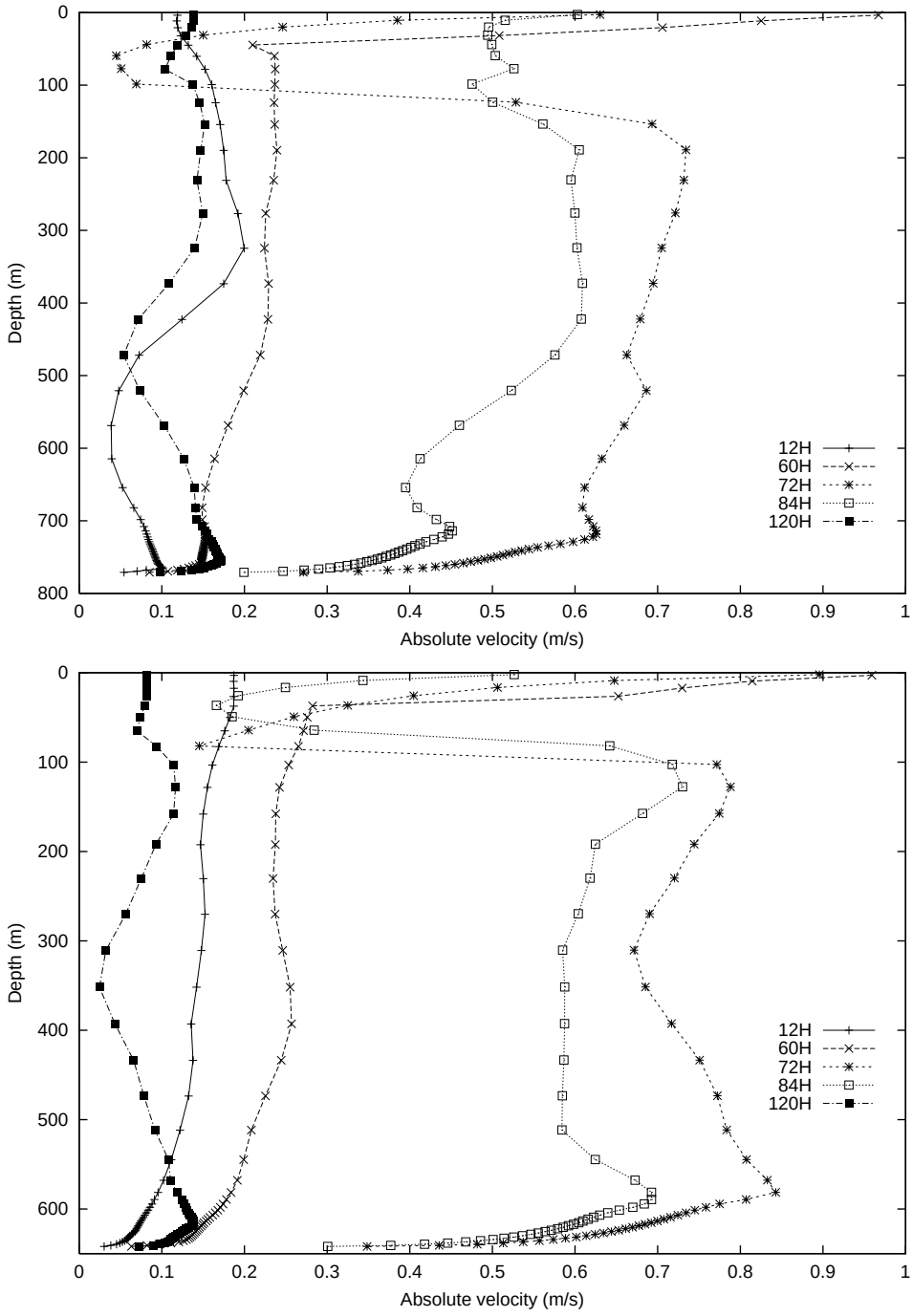


Figure 8: Time evolution of vertical profile for absolute velocity at TP9(top) and TP15(bottom)

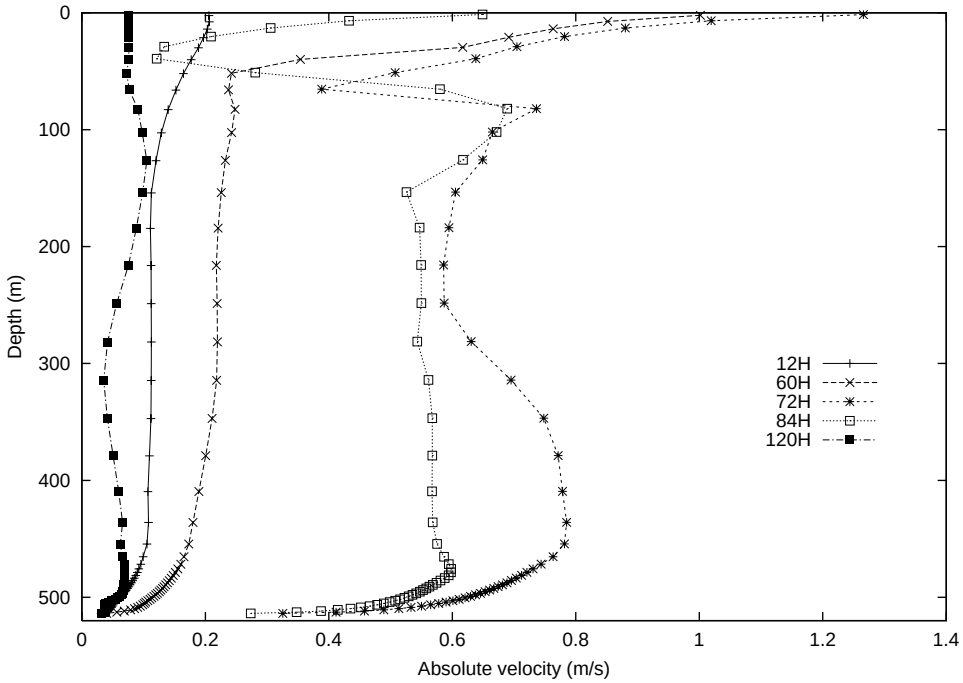


Figure 9: Time evolution of vertical profile for absolute velocity at TP19

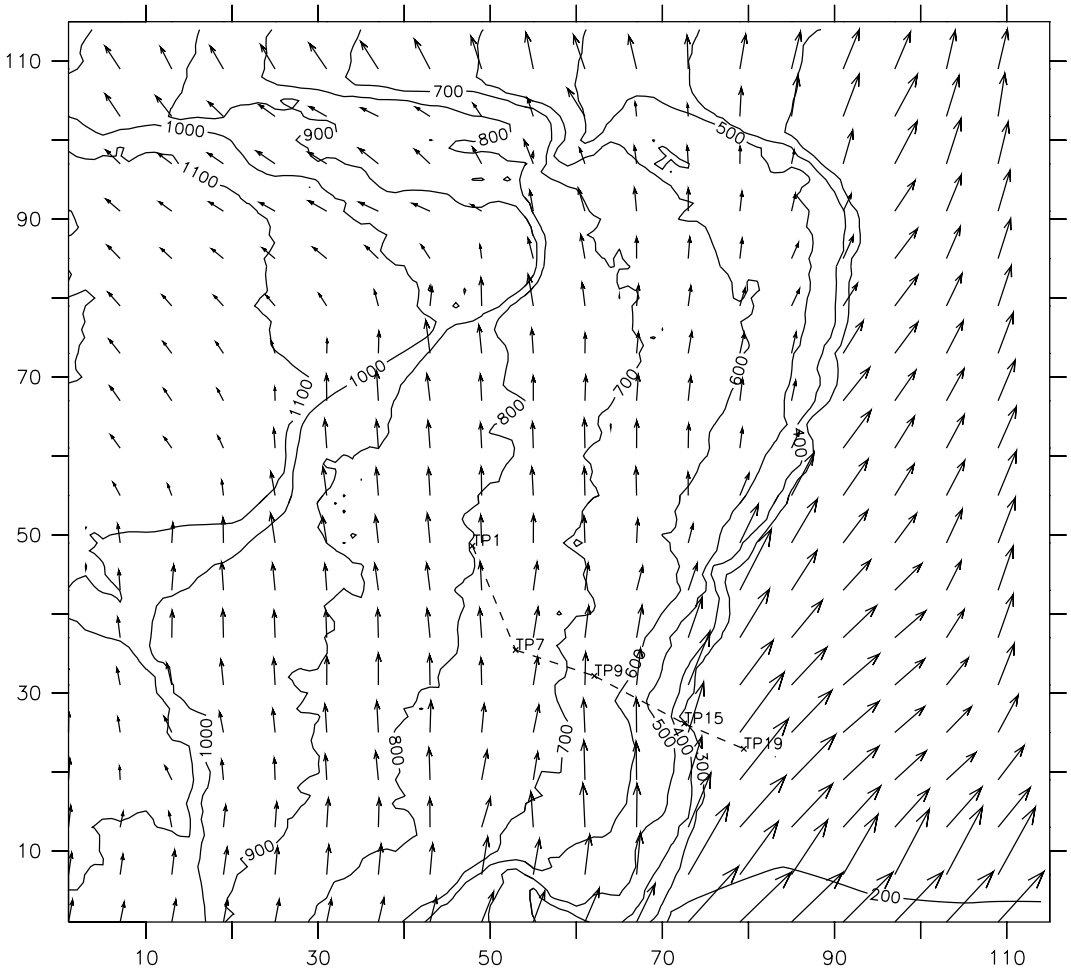


Figure 10: Velocity 5 meter above the bottom after 72 hours. The five stations TP1,TP7,TP9,TP15, and TP19 marked with crosses and a connected line. Axis units are in grid coordinates, grid spacing is 400m in both directions. The longest arrow indicate a velocity equal to 1.26 m/s

Table 2: Direction and magnitude probability at station 1 for velocity at 2 meters depth

cm/s	0°-30°	30°-60°	60°-90°	90°-120°	120°-150°	150°-180°	180°-210°	210°-240°	240°-270°	270°-300°	300°-330°	330°-360°
0- 5	3.0	0.8	0.2	0.3	0.6	0.5	2.5	4.6	1.9	4.1	9.4	19.6
5-10	0.0	0.0	0.0	0.0	0.0	3.0	2.2	3.2	1.7	0.6	1.9	4.9
10-15	10.1	0.0	0.0	0.0	0.0	0.9	0.0	0.0	0.0	0.0	0.6	1.6
15-20	2.5	0.0	0.0	0.0	0.0	0.0	0.0	0.0	0.0	0.0	0.4	1.5
20-40	9.3	0.0	0.0	0.0	0.0	0.0	0.0	0.0	0.0	0.0	0.0	8.1
40-60	0.0	0.0	0.0	0.0	0.0	0.0	0.0	0.0	0.0	0.0	0.0	0.0
60-80	0.0	0.0	0.0	0.0	0.0	0.0	0.0	0.0	0.0	0.0	0.0	0.0
80-**	0.0	0.0	0.0	0.0	0.0	0.0	0.0	0.0	0.0	0.0	0.0	0.0

Table 3: Direction and magnitude probability at station 1 for velocity at 5 meters depth

cm/s	0°-30°	30°-60°	60°-90°	90°-120°	120°-150°	150°-180°	180°-210°	210°-240°	240°-270°	270°-300°	300°-330°	330°-360°
0- 5	5.7	1.7	0.3	0.4	0.5	0.5	1.1	4.2	1.5	1.8	4.9	13.9
5-10	0.0	0.0	0.0	0.0	0.0	1.6	2.0	4.2	2.9	1.6	5.0	8.0
10-15	6.6	0.0	0.0	0.0	0.0	2.0	0.0	0.0	0.0	0.0	0.0	2.2
15-20	5.1	0.0	0.0	0.0	0.0	0.0	0.0	0.0	0.0	0.0	0.0	1.4
20-40	9.5	0.0	0.0	0.0	0.0	0.0	0.0	0.0	0.0	0.0	0.0	7.4
40-60	1.8	0.0	0.0	0.0	0.0	0.0	0.0	0.0	0.0	0.0	0.0	1.9
60-80	0.0	0.0	0.0	0.0	0.0	0.0	0.0	0.0	0.0	0.0	0.0	0.0
80-**	0.0	0.0	0.0	0.0	0.0	0.0	0.0	0.0	0.0	0.0	0.0	0.0

Table 4: Direction and magnitude probability at station 1 for velocity at 10 meters depth

cm/s	0°-30°	30°-60°	60°-90°	90°-120°	120°-150°	150°-180°	180°-210°	210°-240°	240°-270°	270°-300°	300°-330°	330°-360°
0- 5	8.9	2.9	0.4	0.6	0.6	0.5	0.9	4.1	2.0	0.6	3.2	8.0
5-10	0.5	0.0	0.0	0.0	0.0	1.0	1.9	4.2	3.0	2.9	4.1	10.8
10-15	4.1	0.0	0.0	0.0	0.0	2.4	0.0	0.0	0.0	0.0	0.0	1.5
15-20	2.5	5.1	0.0	0.0	0.0	0.0	0.0	0.0	0.0	0.0	0.0	1.1
20-40	8.6	0.0	0.0	0.0	0.0	0.0	0.0	0.0	0.0	0.0	0.0	6.4
40-60	3.7	0.0	0.0	0.0	0.0	0.0	0.0	0.0	0.0	0.0	0.0	3.5
60-80	0.0	0.0	0.0	0.0	0.0	0.0	0.0	0.0	0.0	0.0	0.0	0.0
80-**	0.0	0.0	0.0	0.0	0.0	0.0	0.0	0.0	0.0	0.0	0.0	0.0

Table 5: Direction and magnitude probability at station 1 for velocity at 20 meters depth

cm/s	0°-30°	30°-60°	60°-90°	90°-120°	120°-150°	150°-180°	180°-210°	210°-240°	240°-270°	270°-300°	300°-330°	330°-360°
0- 5	5.2	2.7	1.4	2.0	1.1	0.6	0.9	4.2	1.6	0.4	2.1	7.5
5-10	3.3	0.9	0.2	0.0	0.0	0.9	1.8	4.1	3.4	3.5	4.3	8.7
10-15	2.0	0.0	0.0	0.0	0.0	2.2	0.0	0.0	0.0	0.0	0.0	1.1
15-20	2.8	6.3	0.0	0.0	0.0	0.1	0.0	0.0	0.0	0.0	0.0	1.0
20-40	7.4	0.5	0.0	0.0	0.0	0.0	0.0	0.0	0.0	0.0	0.0	5.2
40-60	5.6	0.0	0.0	0.0	0.0	0.0	0.0	0.0	0.0	0.0	0.0	4.6
60-80	0.0	0.0	0.0	0.0	0.0	0.0	0.0	0.0	0.0	0.0	0.0	0.0
80-**	0.0	0.0	0.0	0.0	0.0	0.0	0.0	0.0	0.0	0.0	0.0	0.0

Table 6: Direction and magnitude probability at station 7 for velocity at 2 meters depth

cm/s	0°-30°	30°-60°	60°-90°	90°-120°	120°-150°	150°-180°	180°-210°	210°-240°	240°-270°	270°-300°	300°-330°	330°-360°
0- 5	14.6	1.4	1.0	0.3	0.2	1.2	0.9	1.3	1.8	2.1	2.0	4.2
5-10	13.9	4.1	0.0	0.0	1.8	3.9	2.8	0.9	0.0	0.4	1.4	7.1
10-15	1.1	6.6	0.0	0.0	0.0	0.0	0.0	0.0	0.0	0.0	0.0	2.1
15-20	0.7	1.9	0.0	0.0	0.0	0.0	0.0	0.0	0.0	0.0	0.0	2.0
20-40	11.1	0.0	0.0	0.0	0.0	0.0	0.0	0.0	0.0	0.0	0.0	7.2
40-60	0.0	0.0	0.0	0.0	0.0	0.0	0.0	0.0	0.0	0.0	0.0	0.0
60-80	0.0	0.0	0.0	0.0	0.0	0.0	0.0	0.0	0.0	0.0	0.0	0.0
80-**	0.0	0.0	0.0	0.0	0.0	0.0	0.0	0.0	0.0	0.0	0.0	0.0

Table 7: Direction and magnitude probability at station 7 for velocity at 5 meters depth

cm/s	0°-30°	30°-60°	60°-90°	90°-120°	120°-150°	150°-180°	180°-210°	210°-240°	240°-270°	270°-300°	300°-330°	330°-360°
0- 5	10.8	1.7	0.7	0.2	0.3	0.9	0.8	0.7	1.8	2.0	2.0	2.1
5-10	19.2	5.8	0.0	0.0	0.0	0.0	2.4	1.8	0.0	0.4	1.3	4.0
10-15	1.1	2.5	0.0	0.0	0.0	5.3	0.4	0.0	0.0	0.0	0.0	2.5
15-20	0.0	5.8	0.0	0.0	0.0	0.0	0.0	0.0	0.0	0.0	0.0	1.7
20-40	5.6	1.3	0.0	0.0	0.0	0.0	0.0	0.0	0.0	0.0	0.0	6.7
40-60	6.2	0.0	0.0	0.0	0.0	0.0	0.0	0.0	0.0	0.0	0.0	1.9
60-80	0.0	0.0	0.0	0.0	0.0	0.0	0.0	0.0	0.0	0.0	0.0	0.0
80-**	0.0	0.0	0.0	0.0	0.0	0.0	0.0	0.0	0.0	0.0	0.0	0.0

Table 8: Direction and magnitude probability at station 7 for velocity at 10 meters depth

cm/s	0°-30°	30°-60°	60°-90°	90°-120°	120°-150°	150°-180°	180°-210°	210°-240°	240°-270°	270°-300°	300°-330°	330°-360°
0- 5	6.9	2.2	0.8	0.2	0.4	0.7	1.1	0.5	1.8	2.2	1.9	0.5
5-10	22.1	6.5	0.8	0.0	0.0	0.0	0.8	2.4	0.1	0.2	1.2	1.7
10-15	2.4	1.0	0.0	0.0	0.0	4.7	2.0	0.0	0.0	0.0	0.1	3.0
15-20	0.0	7.0	0.0	0.0	0.0	0.0	0.0	0.0	0.0	0.0	0.0	1.6
20-40	3.8	2.5	0.0	0.0	0.0	0.0	0.0	0.0	0.0	0.0	0.0	5.9
40-60	8.0	0.0	0.0	0.0	0.0	0.0	0.0	0.0	0.0	0.0	0.0	2.9
60-80	0.0	0.0	0.0	0.0	0.0	0.0	0.0	0.0	0.0	0.0	0.0	0.0
80-**	0.0	0.0	0.0	0.0	0.0	0.0	0.0	0.0	0.0	0.0	0.0	0.0

Table 9: Direction and magnitude probability at station 7 for velocity at 20 meters depth

cm/s	0-30°	30°-60°	60°-90°	90°-120°	120°-150°	150°-180°	180°-210°	210°-240°	240°-270°	270°-300°	300°-330°	330°-360°
0- 5	4.7	4.2	1.5	0.3	0.5	0.4	1.2	0.5	1.7	2.2	1.9	0.8
5-10	13.9	7.4	2.1	0.0	0.0	0.0	0.4	2.7	0.2	0.2	1.1	3.7
10-15	5.0	2.6	0.0	0.0	0.0	4.0	2.7	0.0	0.0	0.0	0.0	1.8
15-20	0.0	6.8	0.0	0.0	0.0	0.0	0.0	0.0	0.0	0.0	0.0	1.1
20-40	2.2	3.6	0.0	0.0	0.0	0.0	0.0	0.0	0.0	0.0	0.0	5.5
40-60	9.1	0.0	0.0	0.0	0.0	0.0	0.0	0.0	0.0	0.0	0.0	3.5
60-80	0.6	0.0	0.0	0.0	0.0	0.0	0.0	0.0	0.0	0.0	0.0	0.0
80-**	0.0	0.0	0.0	0.0	0.0	0.0	0.0	0.0	0.0	0.0	0.0	0.0

Table 10: Direction and magnitude probability at station 9 for velocity at 2 meters depth

cm/s	0°-30°	30°-60°	60°-90°	90°-120°	120°-150°	150°-180°	180°-210°	210°-240°	240°-270°	270°-300°	300°-330°	330°-360°
0- 5	16.5	4.0	1.2	0.2	0.3	0.3	1.3	2.0	1.1	1.9	2.3	6.5
5-10	8.9	5.4	0.0	0.0	0.0	1.8	3.2	0.4	0.0	0.0	1.7	4.2
10-15	0.0	7.6	0.0	0.0	2.6	2.2	0.0	0.0	0.0	0.0	0.0	2.1
15-20	0.1	2.0	0.0	0.0	0.0	0.0	0.0	0.0	0.0	0.0	1.6	0.7
20-40	11.6	0.0	0.0	0.0	0.0	0.0	0.0	0.0	0.0	0.0	0.0	6.0
40-60	0.0	0.0	0.0	0.0	0.0	0.0	0.0	0.0	0.0	0.0	0.0	0.0
60-80	0.0	0.0	0.0	0.0	0.0	0.0	0.0	0.0	0.0	0.0	0.0	0.0
80-**	0.0	0.0	0.0	0.0	0.0	0.0	0.0	0.0	0.0	0.0	0.0	0.0

Table 11: Direction and magnitude probability at station 9 for velocity at 5 meters depth

cm/s	0-30°	30°-60°	60°-90°	90°-120°	120°-150°	150°-180°	180°-210°	210°-240°	240°-270°	270°-300°	300°-330°	330°-360°
0- 5	12.0	2.0	0.7	0.9	0.1	0.0	1.2	1.5	1.2	1.9	1.4	4.4
5-10	14.8	7.7	0.2	0.0	0.0	0.0	2.5	1.2	0.0	0.0	1.8	4.0
10-15	0.0	6.4	0.0	0.0	1.9	4.3	0.5	0.0	0.0	0.0	0.0	1.9
15-20	0.0	2.7	0.0	0.0	0.0	0.0	0.0	0.0	0.0	0.0	0.0	1.8
20-40	4.4	1.5	0.0	0.0	0.0	0.0	0.0	0.0	0.0	0.0	0.0	7.3
40-60	7.3	0.0	0.0	0.0	0.0	0.0	0.0	0.0	0.0	0.0	0.0	0.2
60-80	0.0	0.0	0.0	0.0	0.0	0.0	0.0	0.0	0.0	0.0	0.0	0.0
80-**	0.0	0.0	0.0	0.0	0.0	0.0	0.0	0.0	0.0	0.0	0.0	0.0

Table 12: Direction and magnitude probability at station 9 for velocity at 10 meters depth

cm/s	0°-30°	30°-60°	60°-90°	90°-120°	120°-150°	150°-180°	180°-210°	210°-240°	240°-270°	270°-300°	300°-330°	330°-360°
0- 5	12.3	1.8	0.7	1.0	0.0	0.0	1.2	1.2	1.2	1.4	2.0	2.6
5-10	14.8	9.0	0.3	0.0	0.0	0.0	0.3	2.3	0.0	0.0	1.5	1.7
10-15	1.0	2.1	0.0	0.0	0.0	3.9	2.5	0.0	0.0	0.0	0.0	2.9
15-20	0.0	6.6	0.0	0.0	0.7	0.9	0.0	0.0	0.0	0.0	0.0	1.6
20-40	2.7	2.6	0.0	0.0	0.0	0.0	0.0	0.0	0.0	0.0	0.0	6.8
40-60	9.1	0.0	0.0	0.0	0.0	0.0	0.0	0.0	0.0	0.0	0.0	1.0
60-80	0.0	0.0	0.0	0.0	0.0	0.0	0.0	0.0	0.0	0.0	0.0	0.0
80-**	0.0	0.0	0.0	0.0	0.0	0.0	0.0	0.0	0.0	0.0	0.0	0.0

Table 13: Direction and magnitude probability at station 9 for velocity at 20 meters depth

cm/s	0°-30°	30°-60°	60°-90°	90°-120°	120°-150°	150°-180°	180°-210°	210°-240°	240°-270°	270°-300°	300°-330°	330°-360°
0- 5	6.8	6.2	1.8	0.3	0.0	0.0	1.3	0.9	1.4	1.2	2.0	1.9
5-10	13.8	8.9	2.6	0.0	0.0	0.0	0.0	2.6	0.0	0.1	1.5	2.3
10-15	1.2	1.8	0.0	0.0	0.0	2.7	3.2	0.2	0.0	0.0	0.0	2.4
15-20	0.0	6.6	0.0	0.0	0.0	1.8	0.0	0.0	0.0	0.0	0.0	1.1
20-40	1.2	3.5	0.0	0.0	0.0	0.0	0.0	0.0	0.0	0.0	0.0	5.9
40-60	9.9	0.0	0.0	0.0	0.0	0.0	0.0	0.0	0.0	0.0	0.0	1.9
60-80	0.9	0.0	0.0	0.0	0.0	0.0	0.0	0.0	0.0	0.0	0.0	0.0
80-**	0.0	0.0	0.0	0.0	0.0	0.0	0.0	0.0	0.0	0.0	0.0	0.0

Table 14: Direction and magnitude probability at station 15 for velocity at 2 meters depth

cm/s	0°-30°	30°-60°	60°-90°	90°-120°	120°-150°	150°-180°	180°-210°	210°-240°	240°-270°	270°-300°	300°-330°	330°-360°
0- 5	20.2	2.6	1.2	1.0	0.4	0.2	1.0	1.1	2.6	1.1	4.4	9.6
5-10	4.1	2.6	0.6	2.8	4.1	3.5	0.9	0.0	0.0	0.0	4.9	6.1
10-15	0.0	0.0	1.5	0.2	0.0	0.0	0.0	0.0	0.0	0.0	1.7	0.0
15-20	0.0	0.7	0.3	0.0	0.0	0.0	0.0	0.0	0.0	0.0	0.5	0.9
20-40	2.8	1.1	0.0	0.0	0.0	0.0	0.0	0.0	0.0	0.0	1.2	4.0
40-60	0.0	0.0	0.0	0.0	0.0	0.0	0.0	0.0	0.0	0.0	0.0	10.2
60-80	0.0	0.0	0.0	0.0	0.0	0.0	0.0	0.0	0.0	0.0	0.0	0.0
80-**	0.0	0.0	0.0	0.0	0.0	0.0	0.0	0.0	0.0	0.0	0.0	0.0

Table 15: Direction and magnitude probability at station 15 for velocity at 5 meters depth

cm/s	0°-30°	30°-60°	60°-90°	90°-120°	120°-150°	150°-180°	180°-210°	210°-240°	240°-270°	270°-300°	300°-330°	330°-360°
0- 5	19.7	2.0	2.3	0.3	0.0	0.0	0.6	0.7	2.7	0.5	4.4	8.3
5-10	5.7	2.7	0.1	0.0	2.4	2.5	2.4	0.0	0.0	0.0	1.3	10.6
10-15	0.0	0.0	1.5	2.3	1.6	0.0	0.3	0.0	0.0	0.0	0.0	1.6
15-20	0.0	0.3	0.6	0.0	0.0	0.0	0.0	0.0	0.0	0.0	0.0	1.3
20-40	1.2	1.6	0.0	0.0	0.0	0.0	0.0	0.0	0.0	0.0	0.0	5.6
40-60	1.6	0.0	0.0	0.0	0.0	0.0	0.0	0.0	0.0	0.0	0.0	11.2
60-80	0.0	0.0	0.0	0.0	0.0	0.0	0.0	0.0	0.0	0.0	0.0	0.0
80-**	0.0	0.0	0.0	0.0	0.0	0.0	0.0	0.0	0.0	0.0	0.0	0.0

Table 16: Direction and magnitude probability at station 15 for velocity at 10 meters depth

cm/s	0°-30°	30°-60°	60°-90°	90°-120°	120°-150°	150°-180°	180°-210°	210°-240°	240°-270°	270°-300°	300°-330°	330°-360°
0- 5	17.2	1.9	1.5	0.0	0.0	0.0	0.6	0.6	2.7	0.8	2.6	11.4
5-10	7.4	2.6	0.0	0.0	0.0	1.5	2.7	0.0	0.0	0.0	0.2	11.1
10-15	0.8	0.1	1.3	1.4	3.8	1.2	0.6	0.0	0.0	0.0	0.0	1.6
15-20	0.0	0.1	0.7	0.0	0.0	0.0	0.0	0.0	0.0	0.0	0.0	1.1
20-40	0.5	1.8	0.0	0.0	0.0	0.0	0.0	0.0	0.0	0.0	0.0	5.6
40-60	2.6	0.0	0.0	0.0	0.0	0.0	0.0	0.0	0.0	0.0	0.0	4.0
60-80	0.0	0.0	0.0	0.0	0.0	0.0	0.0	0.0	0.0	0.0	0.0	7.7
80-**	0.0	0.0	0.0	0.0	0.0	0.0	0.0	0.0	0.0	0.0	0.0	0.0

Table 17: Direction and magnitude probability at station 15 for velocity at 20 meters depth

cm/s	0°-30°	30°-60°	60°-90°	90°-120°	120°-150°	150°-180°	180°-210°	210°-240°	240°-270°	270°-300°	300°-330°	330°-360°
0- 5	16.8	2.9	0.3	0.0	0.0	0.0	0.8	0.4	0.6	3.1	0.6	9.4
5-10	10.3	1.7	0.0	0.0	0.0	1.9	3.0	0.0	0.0	0.0	0.0	12.2
10-15	2.0	0.8	1.0	0.0	5.3	0.6	0.0	0.0	0.0	0.0	0.0	1.6
15-20	0.0	0.3	0.4	0.0	0.0	0.0	0.0	0.0	0.0	0.0	0.0	1.1
20-40	0.1	1.9	0.0	0.0	0.0	0.0	0.0	0.0	0.0	0.0	0.0	5.0
40-60	2.8	0.0	0.0	0.0	0.0	0.0	0.0	0.0	0.0	0.0	0.0	2.6
60-80	0.8	0.0	0.0	0.0	0.0	0.0	0.0	0.0	0.0	0.0	0.0	9.5
80-**	0.0	0.0	0.0	0.0	0.0	0.0	0.0	0.0	0.0	0.0	0.0	0.0

Table 18: Direction and magnitude probability at station 19 for velocity at 2 meters depth

cm/s	0°-30°	30°-60°	60°-90°	90°-120°	120°-150°	150°-180°	180°-210°	210°-240°	240°-270°	270°-300°	300°-330°	330°-360°
0- 5	15.2	14.5	3.6	1.6	1.7	2.1	7.1	1.8	0.0	0.0	0.0	11.9
5-10	4.7	2.3	0.2	0.0	0.0	0.0	0.0	0.0	0.0	0.0	1.8	5.3
10-15	0.0	1.4	0.0	0.0	0.0	0.0	0.0	0.0	0.0	0.0	0.0	3.1
15-20	0.0	1.2	0.0	0.0	0.0	0.0	0.0	0.0	0.0	0.0	0.0	0.8
20-40	11.1	0.1	0.0	0.0	0.0	0.0	0.0	0.0	0.0	0.0	0.0	0.8
40-60	7.8	0.0	0.0	0.0	0.0	0.0	0.0	0.0	0.0	0.0	0.0	0.0
60-80	0.0	0.0	0.0	0.0	0.0	0.0	0.0	0.0	0.0	0.0	0.0	0.0
80-**	0.0	0.0	0.0	0.0	0.0	0.0	0.0	0.0	0.0	0.0	0.0	0.0

Table 19: Direction and magnitude probability at station 19 for velocity at 5 meters depth

cm/s	0°-30°	30°-60°	60°-90°	90°-120°	120°-150°	150°-180°	180°-210°	210°-240°	240°-270°	270°-300°	300°-330°	330°-360°
0- 5	16.5	12.7	0.6	1.2	0.6	0.4	2.8	2.3	1.0	0.0	0.1	8.6
5-10	6.3	2.5	0.8	0.0	0.8	2.3	2.8	0.0	0.0	0.0	1.2	8.1
10-15	0.0	1.6	0.0	0.0	0.0	0.0	0.0	0.0	0.0	0.0	0.0	3.5
15-20	0.0	1.0	0.0	0.0	0.0	0.0	0.0	0.0	0.0	0.0	0.0	1.4
20-40	4.6	0.9	0.0	0.0	0.0	0.0	0.0	0.0	0.0	0.0	0.0	1.0
40-60	14.7	0.0	0.0	0.0	0.0	0.0	0.0	0.0	0.0	0.0	0.0	0.0
60-80	0.0	0.0	0.0	0.0	0.0	0.0	0.0	0.0	0.0	0.0	0.0	0.0
80-**	0.0	0.0	0.0	0.0	0.0	0.0	0.0	0.0	0.0	0.0	0.0	0.0

Table 20: Direction and magnitude probability at station 19 for velocity at 10 meters depth

cm/s	0°-30°	30°-60°	60°-90°	90°-120°	120°-150°	150°-180°	180°-210°	210°-240°	240°-270°	270°-300°	300°-330°	330°-360°
0- 5	16.3	8.9	0.0	0.0	0.0	0.4	3.5	0.4	0.8	2.0	0.3	7.1
5-10	10.0	2.3	0.0	0.6	1.7	3.3	1.7	0.0	0.0	0.0	1.0	8.8
10-15	0.4	1.5	0.0	0.0	0.0	0.0	0.0	0.0	0.0	0.0	0.0	3.9
15-20	0.0	0.9	0.0	0.0	0.0	0.0	0.0	0.0	0.0	0.0	0.0	1.9
20-40	3.0	1.2	0.0	0.0	0.0	0.0	0.0	0.0	0.0	0.0	0.0	1.3
40-60	14.1	0.0	0.0	0.0	0.0	0.0	0.0	0.0	0.0	0.0	0.0	0.0
60-80	2.6	0.0	0.0	0.0	0.0	0.0	0.0	0.0	0.0	0.0	0.0	0.0
80-**	0.0	0.0	0.0	0.0	0.0	0.0	0.0	0.0	0.0	0.0	0.0	0.0

Table 21: Direction and magnitude probability at station 19 for velocity at 20 meters depth

cm/s	0°-30°	30°-60°	60°-90°	90°-120°	120°-150°	150°-180°	180°-210°	210°-240°	240°-270°	270°-300°	300°-330°	330°-360°
0- 5	12.3	2.3	0.0	0.0	0.0	0.6	4.6	0.4	0.3	0.7	2.5	5.7
5-10	18.1	1.6	0.0	0.0	1.6	3.8	0.0	0.0	0.0	0.0	0.4	9.0
10-15	4.3	1.4	0.0	0.0	0.0	0.0	0.0	0.0	0.0	0.0	0.0	3.0
15-20	1.3	0.8	0.0	0.0	0.0	0.0	0.0	0.0	0.0	0.0	0.0	1.1
20-40	2.8	1.5	0.0	0.0	0.0	0.0	0.0	0.0	0.0	0.0	0.0	1.5
40-60	10.1	0.0	0.0	0.0	0.0	0.0	0.0	0.0	0.0	0.0	0.0	0.0
60-80	7.9	0.0	0.0	0.0	0.0	0.0	0.0	0.0	0.0	0.0	0.0	0.0
80-**	0.0	0.0	0.0	0.0	0.0	0.0	0.0	0.0	0.0	0.0	0.0	0.0

we see the effect of the boundary layer, with a probability of higher velocities at larger distances from the bottom.

4 Conclusions

In this report we have investigated the effects of the passage of a very strong, idealized low pressure system over the North Sea on the flow around the Ormen Lange production site.

The study has been done by setting up a fine resolution model of an area with an extent of a few tens of kilometers, covering the production site and parts of the pipeline, as well as important topographical features such as the Storegga edge.

The horizontal resolution is high for an ocean model of this kind, but still does not resolve small scale topography that will have important effects on measured data. The report therefore mainly describes the effect of larger scale topography.

The model boundary conditions were produced with a basin scale model with 20km resolution. The model system was set up to simulate the passage of a strong idealized low pressure system over the Norwegian seas. The strength and extent of the low pressure system were chosen on the basis of results from a report by Vikebø et al. where the chosen passage was found to generate the strongest currents along the shelf break.

Simple statistics from the extreme event are presented. As expected the event can clearly be seen in the density function and cumulative distribution for absolute velocity. We also identify the effect of the bottom boundary layer, and observe that the storm is influencing the flow all the way through the boundary layer.

The direction of the flow has large variability before and after the event, while during the event the direction is clearly steered, mainly by the wind direction, but also to some extent by large topographical features.

Generating statistics from one single event gives us distributions like the ones presented in this report, where the event can be seen as an abnormal tail in the probability density distribution. It is likely that a distribution more similar to e.g. the Weibull distribution would be obtained if a Monte Carlo type of simulation were done, using a large number of forcings drawn from distributions of more realistic storms and density fields.

The climatology used in the study is too smooth compared with real data. By doing simulations with sufficiently low viscosity, we might also discover extreme events related to non-linear interactions between waves and density fields with sharper fronts.

Acknowledgements

This work has been supported by Norsk Hydro under contract number 5172100.

The author(s) wish to acknowledge use of the Ferret program for analysis and graphics in this report. Ferret is a product of NOAA's Pacific Marine Environmental Laboratory. (Information is available at http://www.ferret.noaa.gov)

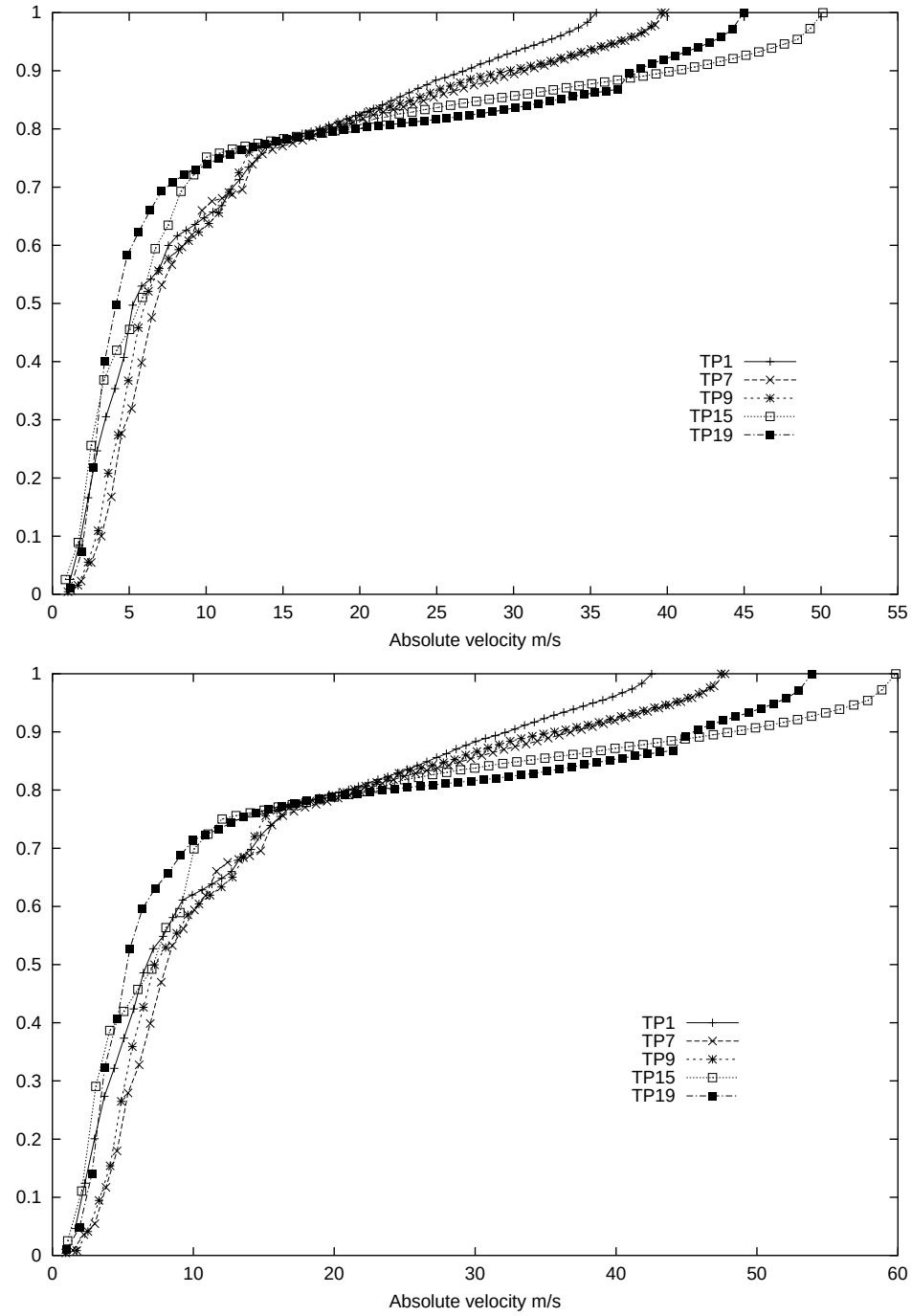


Figure 11: Cumulative distribution of absolute velocity at the five stations for 2m and 5m depth.

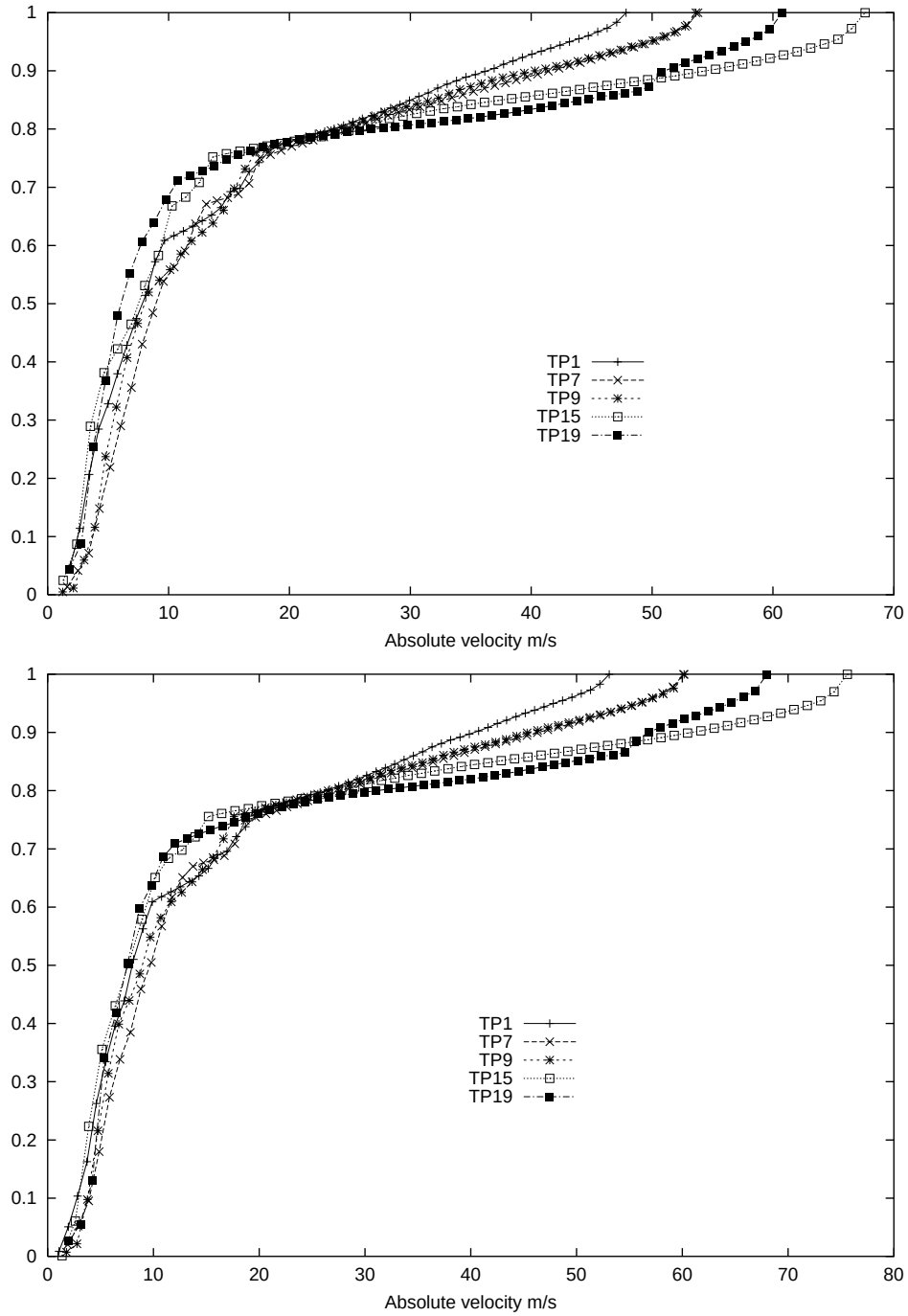


Figure 12: Cumulative distribution of absolute velocity at the five stations for 10m and 20m depth.

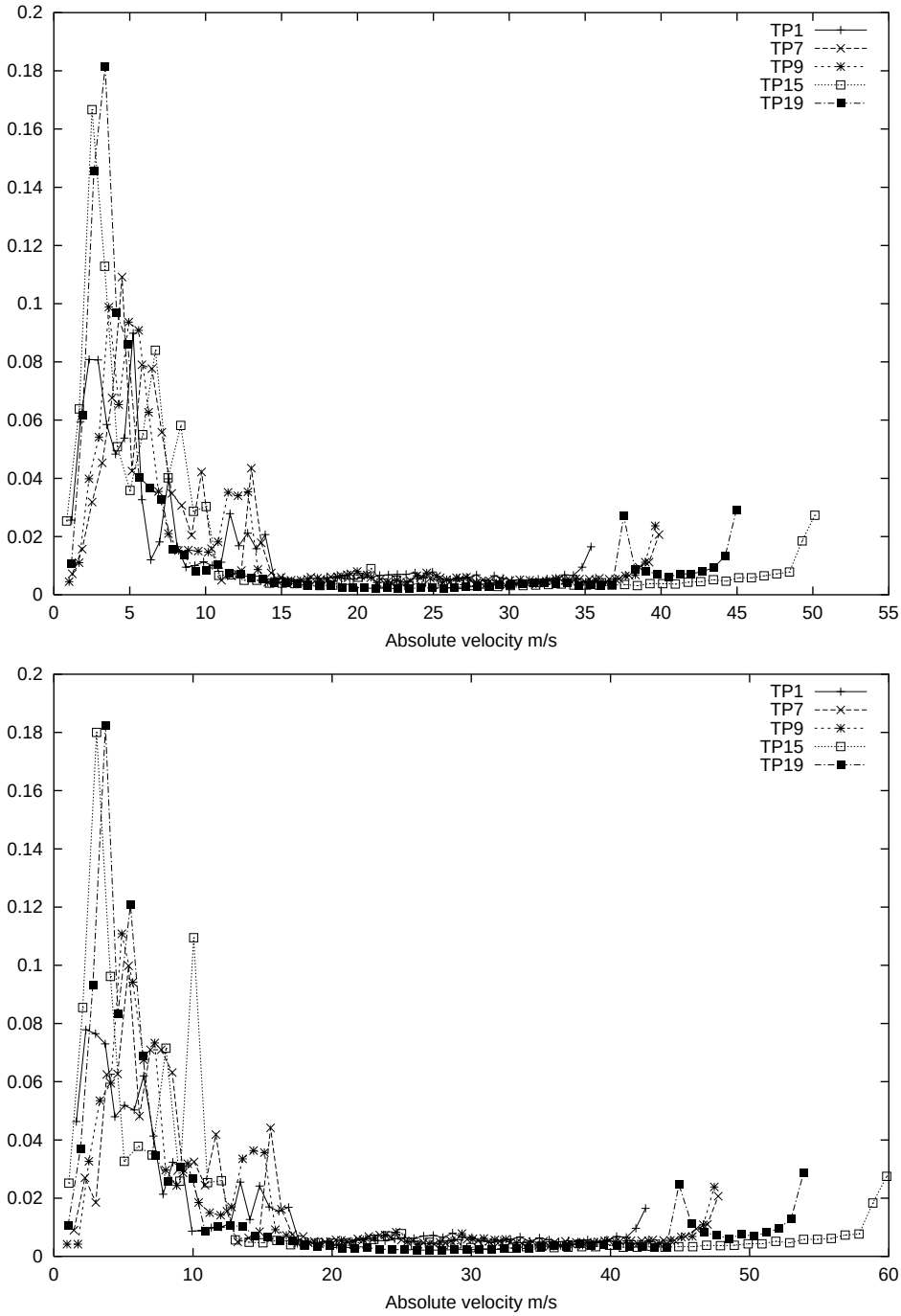


Figure 13: Probability distribution of absolute velocity at the five stations for 2m and 5m depth.

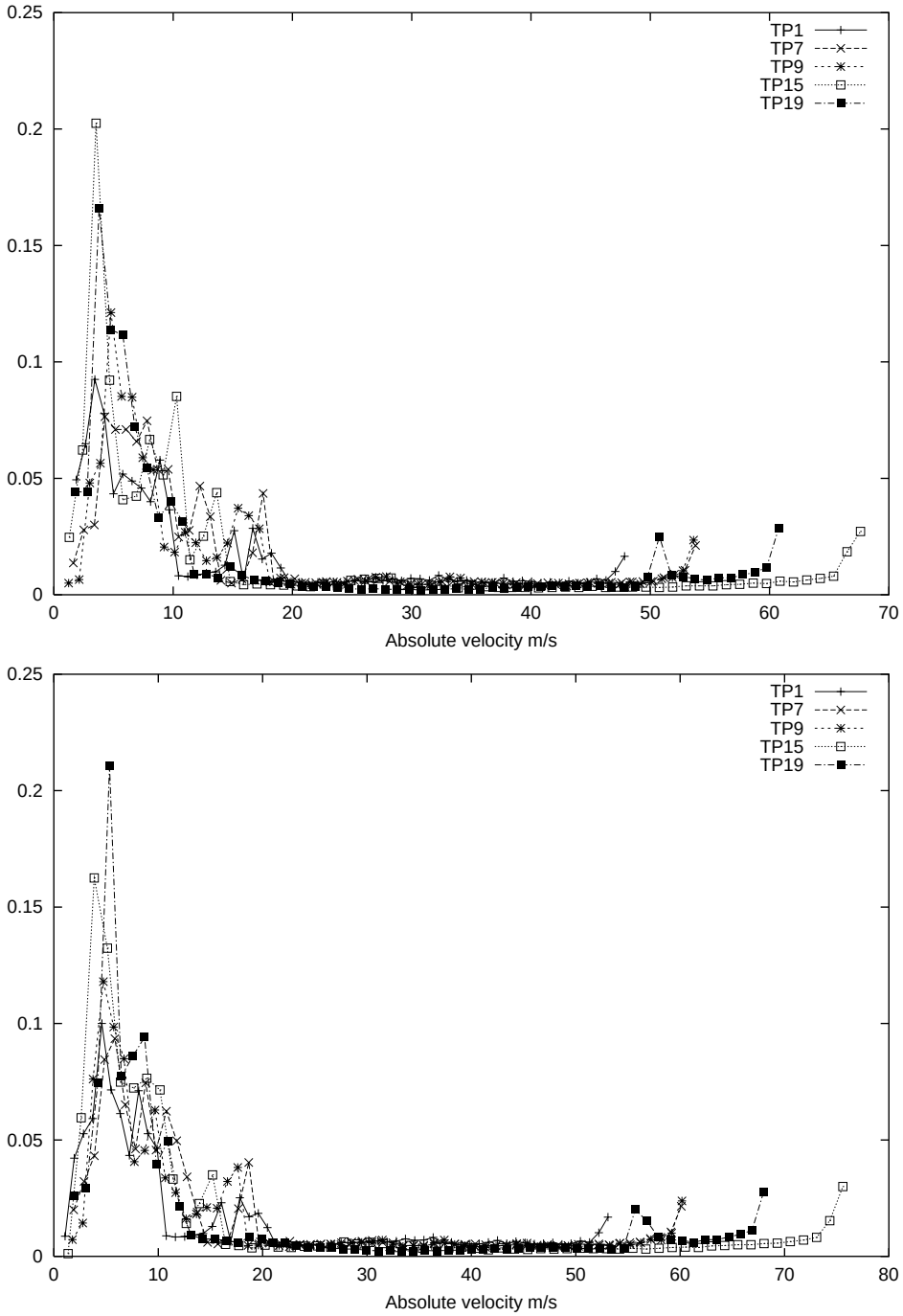


Figure 14: Probability distribution of absolute velocity at the five stations for 10m and 20m depth.

References

[1] J. Berntsen. Users guide for a modesplit σ-coordinate numerical ocean model. version 1.0. Technical Report 135, Department of Applied Mathematics, University of Bergen, 2000.

[2] T. Eldevik, I.K. Eliassen, J. Berntsen, and G. Furnes. On the influence of the thermohaline circulation at Ormen Lange. Technical report, Bergen, May 2001.

[3] I.K. Eliassen. A numerical simulation of the local response of currents at Ormen Lange to a travelling storm. Technical Report CMR-01-A50005, Christian Michelsen Research, Bergen, 2001.

[4] I.K. Eliassen and J. Berntsen. Using a σ-coordinate numerical ocean model for simulating the circulation at Ormen Lange. Technical Report 138, Department of Mathematics, University of Bergen, January 2000.

[5] I.K. Eliassen, T. Eldevik, J. Berntsen, and G. Furnes. The current conditions at Ormen Lange - Storegga. November 2000.

[6] H. Engedahl, B. Ådlandsvik, and E. Martinsen. Production of monthly mean climatological archives of salinity, temperature, current and sea level for the nordic seas. *Journal of Marine Systems*, 14:1–26, 1998.

[7] A.E. Gill. *Atmosphere-Ocean Dynamics*. Academic Press, 1982. ISBN-0-12-283520-4.

[8] D.R. Lynch, J.T.C. Ip, C.E. Naimie, and F.E. Werner. Convergence studies of tidally-rectified circulation on Georges Bank. In American Geophysical Union, editor, *Quantitative Skill Assessment for Coastal Ocean Models*. American Geophysical Union, 1994.

[9] E.A. Martinsen and H. Engedahl. Implementation and testing of a lateral boundary scheme as an open boundary condition in a barotropic ocean model. *Coastal Engineering*, 11:603–627, 1987.

[10] E.A. Martinsen, B. Gjevik, and L.P. Røed. A numerical model for long barotropic waves and storm surges along the western coast of Norway. *J.Phys.Oceanogr.*, 9:1126–1138, 1979.

[11] A. Stigebrandt. Barotropic and baroclinic response of a semi-enclosed basin to barotropic forcing of the sea. In H.J. Freeland, D.M. Farmer, and C.D. Levings, editors, *Proceeding of the NATO Conference on Fjord Oceanography*. Plenum Press, New York, 1980.

[12] F. Vikebø, J. Berntsen, and G. Furnes. Numerical studies of the current response at Ormen Lange to a travelling storm. Technical Report 162, Department of Mathematics, University of Bergen, 2001.